PROCYON B: OUTSIDE THE IRON BOX

J. L. PROVENCAL,[1,2] H. L. SHIPMAN,[1] DETLEV KOESTER,[3] F. WESEMAEL,[4] AND P. BERGERON[4]
Received 2001 October 23; accepted 2001 November 19

ABSTRACT

Procyon B is one of a select group of white dwarf stars in visual binaries that are used to put stringent constraints on the fundamental physics of stellar degeneracy. We present Space Telescope Imaging Spectrograph observations of this elusive white dwarf. Our spectra cover 1800–10000 Å and contain carbon Swan bands, Mg II, and numerous iron features. Procyon B is therefore a rare DQZ white dwarf. Our analysis of the spectrum yields an effective temperature of 7740 ± 50 K and a radius of $0.01234 \pm 0.00032\ R_\odot$. We discuss the implications of these results on observational support for the white dwarf mass-radius relation.

Subject headings: stars: individual (Procyon B) — white dwarfs

1. INTRODUCTION

Every star will meet one of three ends as it approaches the limits of its evolution. If the star is massive, the events triggered by the exhaustion of nuclear fuel in the stellar core will lead to a black hole. If the star is of intermediate mass, the product will be a neutron star. If the star is of low mass, a definition that includes over 90% of all stars currently on the main sequence, the end product will be an electron-degenerate white dwarf.

White dwarfs play important roles in the evolution of the Galaxy and the universe. The structure and composition of white dwarfs contain the records of the final stages of stellar evolution. As they evolve through the planetary nebula phase, pre–white dwarfs inject large quantities of processed material into the interstellar medium. The chemical evolution of the Galaxy is traced through subsequent generations of stars formed from this contaminated material. The white dwarf mass distribution and the luminosity function are used to examine the Galaxy's overall formation history. Type I supernovae, in which an accreting white dwarf undergoes a thermonuclear event, are used as distance indicators demonstrating the acceleration of the universe.

The theoretical mass-radius relation for white dwarfs is a generally accepted underlying assumption in all studies of white dwarfs and their properties. The theory predicts the radius of a white dwarf of given mass and interior composition, usually assumed to contain a mixture of carbon and oxygen. An important consequence of the mass-radius relation is the limiting mass for white dwarfs (Chandrasekhar 1933), above which an object cannot be supported by electron degeneracy and must become either a neutron star or a black hole. One would like to assume that as fundamental a theory as the white dwarf mass-radius relation rests on solid observational grounds. Figure 1 displays the observational support for this relation circa 1997.

We are engaged in an ongoing project to improve the observational underpinnings for this basic theory. At first glance, this goal seems uncomplicated, because we require only independent observations of white dwarf masses and radii. The dilemma with observational results hinges on the word "independent." Determinations of masses and radii in ways that do not invoke the mass-radius relation are quite difficult. Problems include a lack of well-defined parallaxes and effective temperatures required for radius measurements. The *Hipparcos* Space Astrometry mission, with its limiting magnitude of ∼12, is unable to provide parallaxes for faint white dwarfs (see Provencal et al. 1998 for a detailed discussion). The best test of stellar degeneracy remains the determination of radii for white dwarfs in nearby visual binaries. In these cases, masses are well determined from orbital parameters, and stellar radii can be derived from known parallaxes and knowledge of effective temperatures.

Procyon B is a member of this select group of white dwarfs. It is the third brightest white dwarf known and has a well-determined mass, $M = 0.602 \pm 0.015\ M_\odot$, and distance, $d = 3.50 \pm 0.01$ pc (Girard et al. 2000). Unfortunately, nature has conspired to place this object $5''$ from one of the brightest stars in our sky. Until recently, little was known concerning the white dwarf's surface temperature and atmospheric composition. In 1995, we obtained a series of WFPC2 images of the Procyon system, with the goal of determining those parameters (Provencal et al. 1997). In brief, the WFPC2 photometric observations suggested a helium-rich atmosphere consistent with $T_{\rm eff} = 8688 \pm 200$ K. This determination resulted in a stellar radius of $0.0096 \pm 0.0005\ R_\odot$ (Provencal et al. 1997).

Figure 1 provides convincing evidence that further study of Procyon B is warranted. If we assume that Procyon B is a normal white dwarf, the results of Provencal et al. (1997) argue for a reconsideration of the mass-radius relation, because the position of Procyon B lies several sigma from the expected value for carbon-core white dwarfs. On the other hand, if we accept the mass-radius relation, as argued by observations of 40 Eri B and Sirius B, our WFPC2 results indicate that Procyon B has a core as heavy as iron, rather than the commonly assumed carbon core; this is the "iron box" referred to by Shipman & Provencal (1999). Since either option represents a distinct challenge to currently accepted ideas, our understanding of white dwarf and binary evolution would greatly benefit from revisiting this

[1] Department of Physics and Astronomy, University of Delaware, Newark, DE 19716; jlp@udel.edu.

[2] Resident Astronomer, Mount Cuba Observatory.

[3] Institut für Astronomie und Astrophysik, Universität Kiel, D-24098, Kiel, Germany; koester@astrophysik.uni-kiel.de.

[4] Département de Physique, Université de Montréal, C.P. 6128, Succursale Centre-Ville, Montreal, QC H3C 3J7, Canada; wesemael@astro.umontreal.ca, bergeron@astro.umontreal.ca.
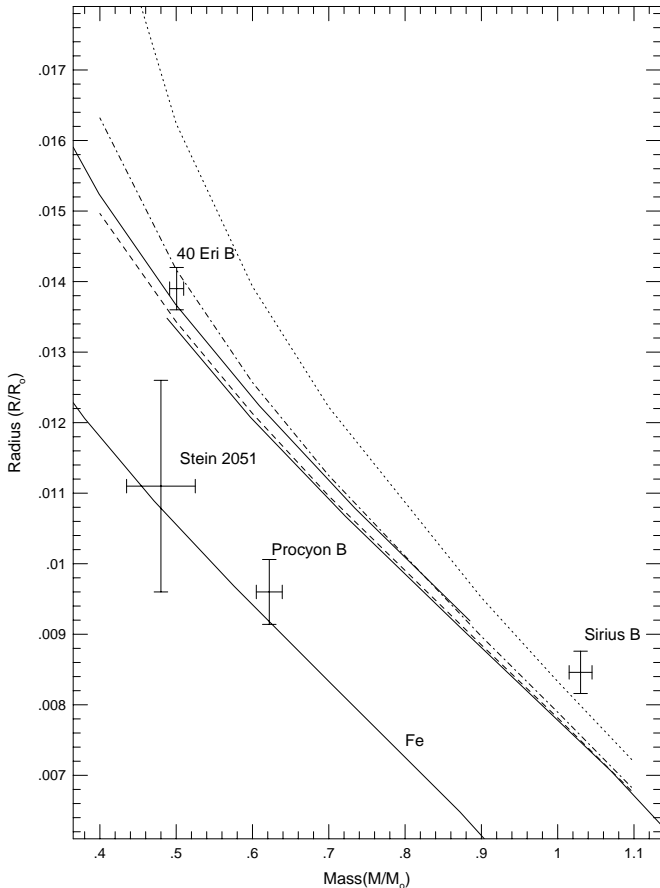
FIG. 1.—Observational support for the mass-radius relation circa 1997. The solid lines represent zero-temperature Hamada & Salpeter (1961) relations for He, C, and Fe core compositions. The remaining sequences shown are from Wood (1995) and contain carbon cores. The dotted line is a $T_{eff} = 25,000$ K white dwarf with $M_{He} = 10^{-2}$ and $M_H = 10^{-4}$. The dot-dashed line and the dashed line are for $T_{eff} = 16,700$ and 7800 K, respectively. They consist of carbon cores surrounded by helium envelopes with $M_{He} = 10^{-4}$. The error bars indicate 1 σ errors in mass and radius.

problem. With these ideas in mind, we secured Cycle 7 Space Telescope Imaging Spectrograph (STIS) time to obtain spectra of Procyon B and reexamine the issue of Procyon B's radius in some detail.

2. OBSERVATIONS AND REDUCTION

We obtained STIS observations of Procyon B at low and medium resolution. The proximity of our target to Procyon A makes acquisition of the white dwarf complicated. The experience gained during a previous attempt with the Faint Object Spectrograph (FOS) forced us to three compromises in our acquisition procedure. First, we calculated an offset from Procyon A, based on STIS images obtained one month before our spectroscopic observations. This could not be done with the FOS because of Procyon A's extreme brightness. Second, we could not predict the results of attempting to center Procyon B in the STIS slit because of the high background. *HST* did not report a target acquisition failure during our previous FOS observations, but it apparently acquired an artifact from Procyon A. We concluded that our knowledge of Procyon B's position was accurate enough to offset from Procyon A and put the white dwarf in the slit without centering. This decision led to our third

compromise. We elected to use the larger $52'' \times 0''.2$ slit to ensure the presence of the white dwarf.

The spectra cover 1700–10200 Å, using a variety of gratings (Table 1). The reduction process follows the standard pipeline until the final extraction of the one-dimensional spectra. Figure 2 displays the two-dimensional spectrum for observation o4g802010 (see Table 1). The white dwarf is not centered in the slit, and contamination from Procyon A is evident. Figure 3 presents the gross counts versus the background for the three low-resolution observations (Table 1). In each case, the background is 4% of the gross flux. We carefully examined background subtraction from various locations. Our best results were obtained using background extraction boxes 5 pixels wide, offset ± 12 pixels from the spectrum center.

Our flux accuracy depends on such factors as the size of the aperture used, the scattering of light, and the accuracy to which the source is centered in the slit. Figure 4 shows the combined low- and medium-resolution spectra as they arrive from the calibration pipeline. The UV and optical low-resolution spectra are not on the same absolute scale, resulting in a discontinuity near 3000 Å. For grating G230LB (covering 1680–3060 Å), we find an average flux between 2900 and 3000 Å of 2.70×10^{-13} ergs s^{-1} cm^{-2} Å^{-1}, with a signal-to-noise ratio of 91. For grating G430L (covering 2900–5700 Å), we find an average flux between 2900 and 3000 Å of 2.86×10^{-13} ergs s^{-1} cm^{-2} Å^{-1}, with a signal-to-noise ratio of 25. The fluxes from these two gratings differ by ~6%, within the advertised accuracies of our instrument configuration, especially considering that our target was not well centered in the slit (Fig. 2). However, the medium-resolution spectra (grating G430M), covering a wavelength region similar to G430L's, have an average flux of 2.74×10^{-13} ergs s^{-1} cm^{-2} Å^{-1}, with a signal-to-noise ratio of 90. This agrees much more closely with the flux from G230LB.

Our analysis places considerable weight on the absolute flux level of the energy distribution in the derivation of Procyon B's effective temperature. It is essential (1) to further investigate the internal consistency among the available STIS spectra and (2) to understand to what extent the STIS optical fluxes relate to the WFPC2 broadband photometry used in our previous analysis (Provencal et al. 1997). After several experiments, including comparisons with the WFPC2 photometry, the different STIS spectra, and published magnitudes (Walker et al. 1994), we opted for the following procedure: we apply a gray correction factor *f* to the low-resolution optical data only, a correction factor predominantly determined by the need for internal consistency among the G230LB, G430L, and G430M fluxes. Because the modeling of charge transfer effects (CTE) affecting the WFPC2 data used by Provencal et al. (1997) has substantially improved since our earlier analysis, we looked for no more than a rough agreement with the WFPC2 photometric data given in Table 3 of Provencal et al. (1997). We find that a downward scaling of the low-resolution flux level (G430L) by $f = 0.90$ represents a suitable compromise.

The corrected low-resolution spectrum is given in Figure 5, together with the WFPC2 photometry of Provencal et al. (1997). The most conspicuous features are the carbon Swan bands near 4700 and 5200 Å and the Mg II resonance lines near 2800 Å. At the short-wavelength end of the ultraviolet spectrum, we find the asymmetric C I $\lambda 1930$ line, as well as numerous iron features between 2200 and 2800 Å. The

TABLE 1
JOURNAL OF OBSERVATIONS

| Observation	Grating	Dispersion (Å pixel⁻¹)	Central Wavelength (Å)	Δλ (Å)	Exposure Time (s)
o4g802010......	G230LB	1.35	2375	1380	528.0
o4g8020j0.......	G430L	2.73	4300	2900	18.0
o4g8020k0	G750L	4.92	7751	5030	36.0
o4g802020......	G430M	0.28	3680	286	180.0
o4g802030......	G430M	0.28	4706	286	180.0
o4g802040......	G750M	0.56	7283	570	120.0
o4g802070......	G750M	0.56	9336	570	100.0
o4g802080......	G750M	0.56	5734	570	100.0
o4g802090......	G430M	0.28	3936	286	150.0
o4g8020a0.....	G430M	0.28	3423	286	170.0
o4g8020b0	G430M	0.28	4194	286	180.0
o4g8020c0.....	G750M	0.56	9851	570	120.0
o4g8020d0.....	G750M	0.56	9851	570	180.0
o4g8020e0......	G750M	0.56	10363	570	600.0
o4g8020f0	G750M	0.56	10363	570	280.0
o4g8020g0......	G430M	0.28	5216	286	160.0
o4g8020h0	G430M	0.28	4451	286	180.0
o4g8020i0.......	G750M	0.56	6768	570	108.0
o4g8020m0	G750M	0.56	8825	570	140.0
o4g8020n0	G750M	0.56	8825	570	120.0
o4g8020o0	G430M	0.28	3165	286	300.0
o4g8020p0	G750M	0.56	6252	570	120.0
o4g8020q0	G430M	0.28	4961	286	180.0
o4g8020r0	G740M	0.56	8311	570	120.0
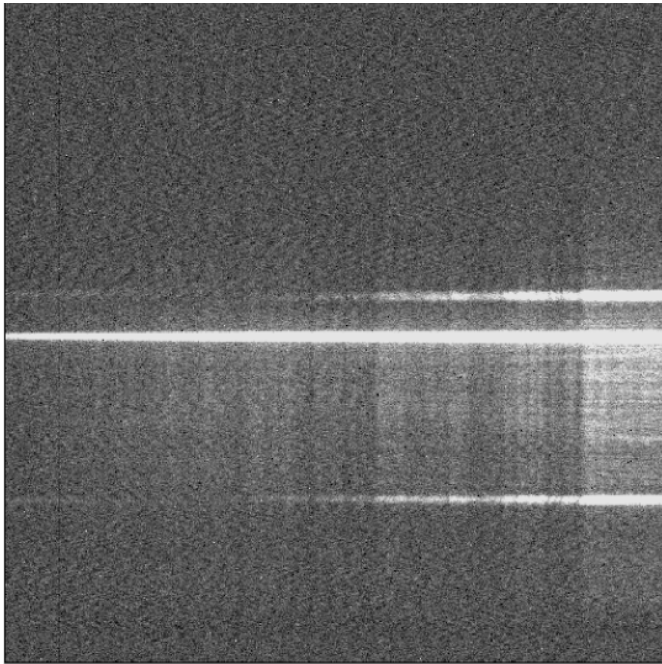
FIG. 2.—Two-dimensional spectrum for observation o4g802010. The CCD chip is 1024 × 1024 pixels with dispersion direction along the x-axis. The bright line extending along the entire x-axis is the spectrum of Procyon B. The two fainter lines above and below the spectrum represent the slit edges illuminated by reflected light. The overall illumination of the slit is due to contamination by Procyon A. The background contamination is much lower than expected. The spectrum is not well centered in the slit.
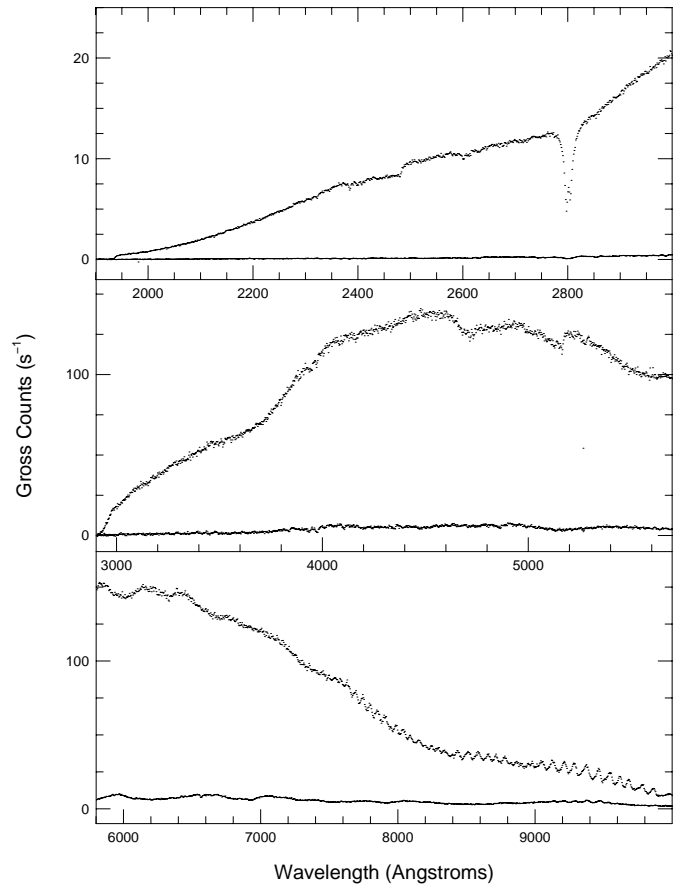

FIG. 3.—Gross vs. background counts for the three low-resolution spectra. The fringing pattern in o4g8020k0 (bottom panel) arises from the interference of the incident beam and light reflected from the substrate of the back-illuminated CCD. This is removed during the final stages of reduction.
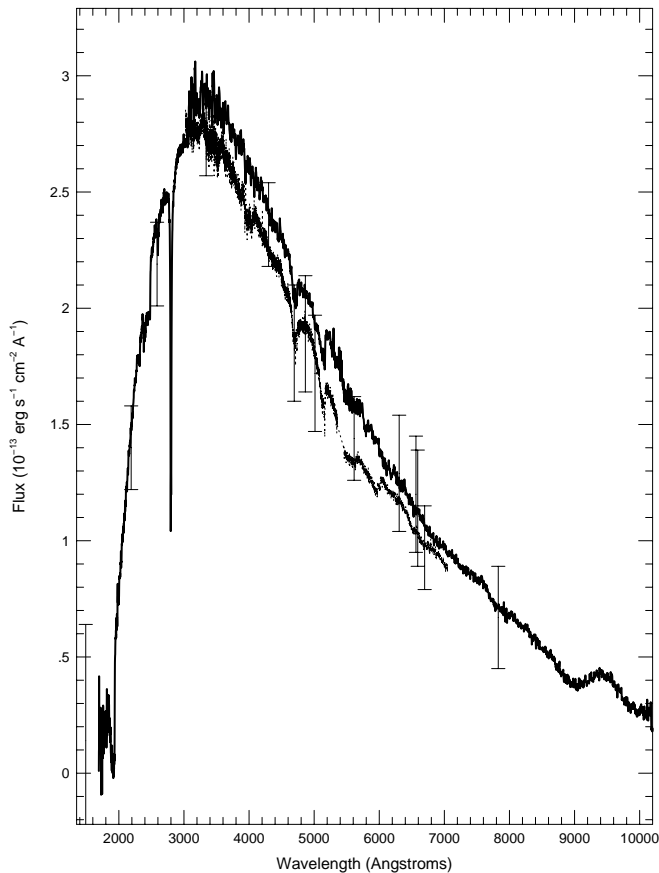
FIG. 4.—STIS low-resolution spectrum (*line*), compared with the medium resolution spectra (*points*) and the WFPC2 photometry (*error bars*) of Provencal et al. (1997). The broad bump at 9000 Å in the low-resolution spectrum is a reduction artifact.
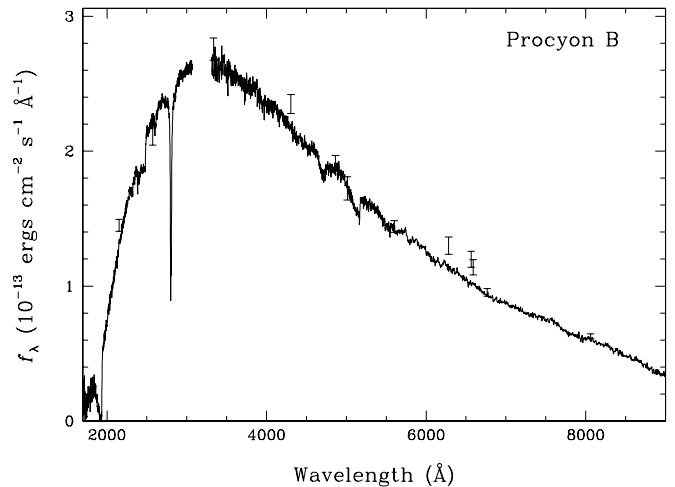

FIG. 5.—Corrected low-resolution spectrum of Procyon B. We exclude the G430L data between 2900 and 3300 Å because they are of lower quality than the remaining data. Note the carbon Swan bands (4700 and 5150 Å) and the Mg II resonance line (2800 Å), as well as the asymmetric C I λ1930 line. The WFPC2 photometry analyzed by Provencal et al. (1997) is also shown, using thick error bars for the broadband filters and thin error bars for the narrowband filters.

medium-resolution spectrum, not displayed here, also shows weak but clear Ca II H and K lines. We find no sign of the Balmer lines. The spectral type of Procyon B is now known: it is a DQZ white dwarf.

3. MODEL ATMOSPHERES

For this updated analysis of Procyon B, we use models generated with the model atmosphere code developed by one of us (D. K.) and described in Finley, Koester, & Basri (1997). Earlier versions of this code are used in the modeling of DQ stars (Koester, Weidemann, & Zeidler-K. T. 1982); its current version is most appropriate for the analysis of Procyon B's spectra, which reveal the presence of both carbon and other heavy elements. We note that our earlier investigation of Procyon B's photometric properties was carried out on the basis of another stellar atmosphere code, also developed by one of us (P. B.). This second code is the basis for recent extensive investigations of the atmospheric properties of cool white dwarfs (Bergeron, Ruiz, & Leggett 1997; Bergeron, Leggett, & Ruiz 2001). At the time of the 1997 analysis, this code, whose basic structure is described by Bergeron, Saumon, & Wesemael (1995), only included hydrogen and helium as atmospheric constituents. This was deemed appropriate at the time, because the dominant atmospheric constituent of Procyon B was unknown.

4. DETERMINATION OF ATMOSPHERIC PARAMETERS

4.1. *Effective Temperature and Carbon Abundance*

The determination of atmospheric parameters for helium-rich white dwarfs can be accomplished in several ways. For objects above ~12,000 K, it is straightforward to compare neutral and/or ionized helium-line profiles with detailed theoretical models, while the ionization balance of various elements (be they helium or some minor constituent) provides additional constraints. For stars cooler than that threshold, the neutral helium lines become spectroscopically invisible, and the temperature (and, in the case of very cool stars below ~4000 K, even the composition) of the atmosphere can only be derived from an examination of the overall flux distribution. For those stars, the strength of occasional lines of heavy elements might provide additional constraints on $T_{\rm eff}$. This is the situation we face with Procyon B, where our spectra span nearly the complete wavelength range with significant flux and allow a determination of the effective temperature.

Accordingly, we use the following relationship among the observed monochromatic flux f_λ, the Eddington flux at the stellar surface H_λ, the stellar radius R, and the distance D:

$$f_\lambda = 4\pi H_\lambda R^2/D^2 = 4\Omega H_\lambda(T_{\rm eff}, \log g, [{\rm C/He}]) , \quad (1)$$

where we have defined the solid angle

$$\Omega \equiv \pi R^2/D^2 . \quad (2)$$

Note that the distance is obtained directly from the trigonometric parallax measurement. Our fitting technique relies on the nonlinear least-squares method of Levenberg-Marquardt (Press et al. 1986), which is based on a steepest-descent method. The expression given by equation (1) is valid at each wavelength, and the value of χ^2 is thus taken as the sum over all wavelengths of the difference between both
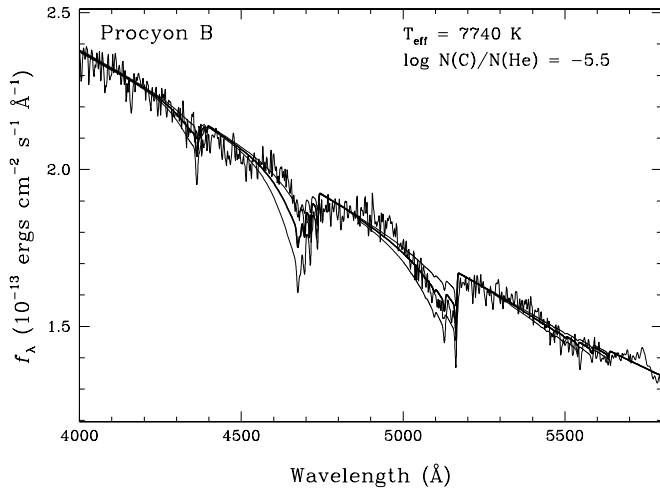
FIG. 6.—Match of our synthetic spectrum, calculated for log[C/He] = −5.5 and convolved with a ∼5 Å instrumental profile, to the low-resolution spectrum of the carbon Swan bands (*thick line*). The models do not quite reproduce the strong curvature between the two bands, especially near 4800 Å. Also shown are two models with log[C/He] = −5.7 and −5.3 (*thin lines*). The carbon abundance seems relatively well constrained by the strength of the molecular bands. The effective temperature used here, $T_{\rm eff}$ = 7740 K, is the optimal temperature derived from the energy distribution.

FIG. 7.—Best fit to the energy distribution of Procyon B. The model has $T_{\rm eff}$ = 7740 K, log *g* = 8.0, and log[C/He] = −5.5. Note the strong C I λ2478 line, which, at that carbon abundance, is predicted to be much stronger than is observed.

sides of the equation. We consider $T_{\rm eff}$, Ω, and [C/He] ≡ N(C)/N(He) free parameters; the formal uncertainties of all parameters are obtained directly from the covariance matrix of the fit. Since the mass of Procyon B is typical of white dwarfs and is known to high accuracy ($M = 0.602 \pm 0.015\ M_\odot$; Girard et al. 2000), we assume log *g* = 8.0 throughout. At first glance, this may seem circular, since log *g* = 8.0 is the value expected at $M \sim 0.6\ M_\odot$ if one assumes that the carbon mass-radius relation is valid. While the surface gravity is indeed dependent on radius, the model fluxes themselves depend only weakly on gravity (Koester & Wolff 2000). The use of log *g* = 8.0 thus does not affect our final estimates.

Our model grid covers the range of 6000 K ≤ $T_{\rm eff}$ ≤ 10,000 K and −8.0 ≤ log[C/He] ≤ −4.0. Our initial attempts at a two-dimensional fit to the complete energy distribution of Procyon B yield estimates of $T_{\rm eff}$ = 7687 K and log[C/He] = −5.8. Next, we attempt a formal fit to the Swan bands in the low-resolution optical spectrum and obtain consistent values of $T_{\rm eff}$ = 7712 K and log[C/He] = −5.6. At that carbon abundance, however, the predicted red band remains weaker than is observed. Even though our model does not predict the strong curvature between the two bands, a slightly higher carbon abundance (log[C/He] = −5.5) clearly gives the correct overall strength for the optical features and seems a more judicious choice. As shown in Figure 6, the optimal carbon abundance is effectively constrained from the optical data, with variations in log[C/He] of ±0.2 leading to clearly unsatisfactory matches to the Swan bands. Accordingly, we adopt the value log[C/He] = −5.5 ± 0.2 for the rest of the analysis.

With the carbon abundance constrained, we fit the energy distribution one final time, finding $T_{\rm eff}$ = 7740 K. The associated solid angle and stellar radius (see below) are $\Omega = 1.989 \times 10^{-20}$ sr and $R = 0.01234\ R_\odot$, respectively. Our best fit to the low-resolution data is displayed in Figure 7. Apart from the 2000–2400 Å range and residual observa-
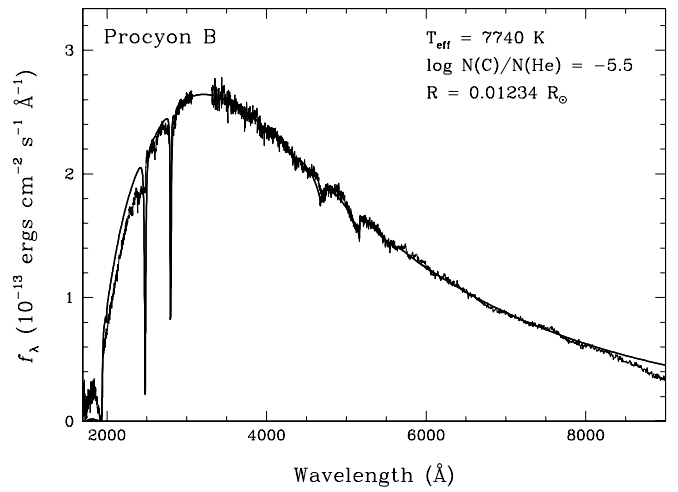
tional fringing effects, the fit to the energy distribution of Procyon B is quite good.

Also present in our data are the ultraviolet lines C I λλ1930 and 2478. C I λ1930 displays an asymmetric profile, given the reality of the flux shortward of 1900 Å (Fig. 8), with negligible absorption in the red wing. C I λ2478 dis-
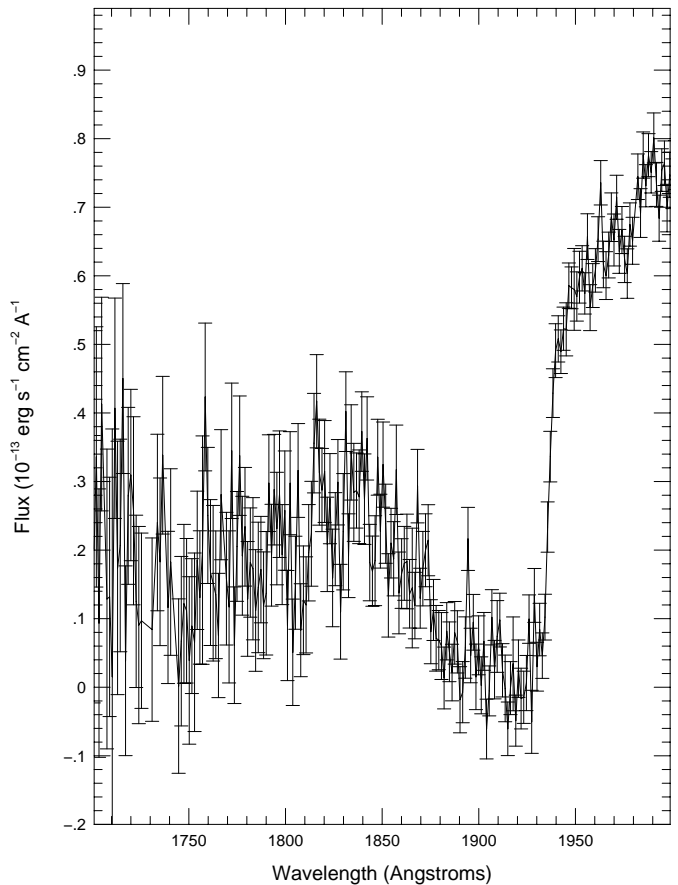

FIG. 8.—Low-resolution spectrum near C I λ1930. We include error estimates for each point to demonstrate the reality of flux shortward of 1900 Å. The observations between 1800 and 1930 Å are significant at the 3.5 σ level.

plays the same steep red edge, but is much weaker than predicted. These problems associated with the C I lines are seen in other DQ white dwarfs (Koester et al. 1982) and are not specific to Procyon B. The strength of the ultraviolet C I lines suggests abundances that are not in agreement with the molecular carbon abundances. In the case of Procyon B, our best fit to the ultraviolet C I lines is $\log[C/He] = -7.0$, a factor of ~ 30 lower than the abundance derived from the molecular Swan bands. This substantial inconsistency in the carbon abundance suggests that our error estimate for the carbon abundance quoted above (± 0.2 dex) may be overly optimistic. However, the fit to the energy distribution obtained using models at a low carbon abundance (not shown here) is significantly worse than that achieved with our optimal value of C/He. It is our feeling that the true uncertainty of $\log[C/He]$ is considerably smaller than the range (-7 to -5.5) discussed here.

Why, then, does this inconsistency arise? The problem most likely originates with our understanding of broadening of C I lines by neutral helium. Conditions in the helium-dominated photospheres of cool white dwarfs are extreme. The neutral particle density in the region of line formation can be as high as 10^{21} cm^{-3}, with gas pressure in excess of 10^9 dynes cm^{-2} at $\tau = 0.1$. The mean interparticle distances are not much larger than the sizes of atoms and molecules. Strong broadening should not come as a surprise.

4.2. *Abundances of Other Elements*

We use the model that best fits the energy distribution and the carbon Swan bands ($T_{\text{eff}} = 7740$ K, $\log[C/He] = -5.5$) to determine the abundances of Mg, Fe, and Ca. Our detailed synthetic spectra include approximately 4000 lines, with data obtained from the Kurucz & Bell (1995) line lists. Our final results are given in Table 2. As an example, Figure 9 shows the fit to the Mg II resonance lines. As is seen in other DZ stars (Zeidler-K. T., Weidemann, & Koester 1986; Wehrse & Liebert 1980 and references therein), the fit to the wings is not particularly good. This problem is most likely due to inadequate broadening theories for these extreme atmospheres, as alluded to above, to explain the differences in carbon abundance derived from atomic and molecular features.

4.3. *Reappraisal of the Provencal et al. (1997) Analysis*

The effective temperature of Procyon B determined here, on the basis of newly acquired STIS spectroscopy and models appropriate for DQ stars, is significantly lower than the ~ 8700 K value derived by Provencal et al. (1997) from the WFPC2 photometry and hydrogen/helium composition model atmospheres. This disagreement prompted us to investigate the internal consistency of the two model grids
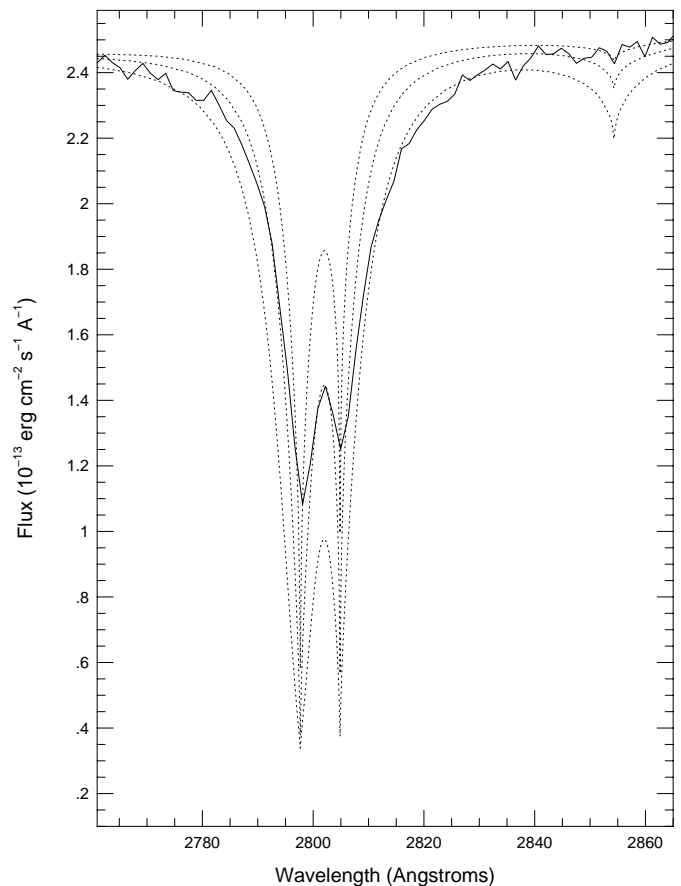

FIG. 9.—Mg II and Mg I lines in the spectrum of Procyon B (*solid line*). We compare with 7740 K models with $[Mg/He] = (2, 4, 8) \times 10^{-11}$ (*dotted lines, from shallowest to deepest*).

for our analysis of Procyon B. Various tests carried out with both codes suggest the following: the effective temperature obtained from a match to the energy distribution is lowered when model atmospheres including additional electron donors (especially carbon, in this case) are used. This is best shown in Figure 10, where we display the energy distributions for several models of interest, all at $T_{\text{eff}} = 7700$ K and $\log g = 8.0$: a pure helium model (akin to the one used in Provencal et al. 1997); a model with traces of carbon, $\log[C/He] = -5.5$; and a model with the same traces of carbon but without the *carbon opacity* included. Even though the effective temperature of all three models is identical, there is a significant shift in the peak of the energy distribution for the models including traces of carbon, *which thus appear bluer than their carbon-free counterparts*. This shift is already apparent in the line-free model. The further inclusion of the carbon transitions causes a small redistribution of the emergent flux, especially around the peak of the energy distribution, but does not further shift the peak's position.

The consequence of this shift can be appreciated from a numerical experiment in which we fit the emergent flux from a 7700 K, $\log g = 8.0$ model photosphere including traces of carbon ($\log[C/He] = -5.5$), as well as carbon lines, with the pure helium model grid. The resulting optimal effective temperature is $T_{\text{eff}} = 8414$ K. This experiment clearly accounts for the discrepancy between the temperatures of Provencal et al. (1997) and our current estimate. When matching against the observed distribution of Procyon B, we expect
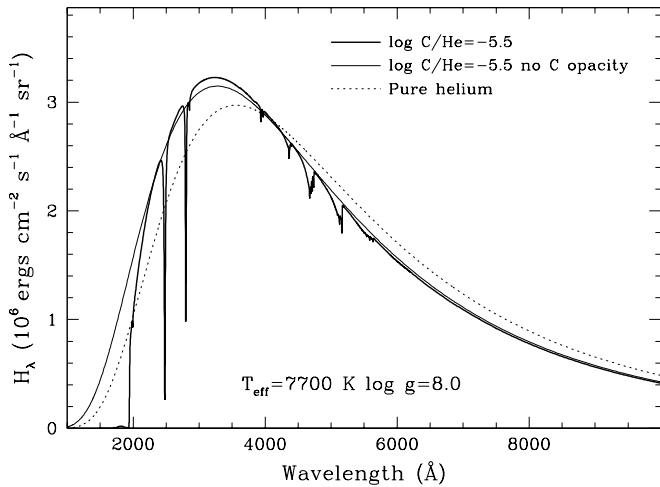
TABLE 2
Element Abundances

Element	log(Element/He) (by number)
Hydrogen......	< -4
Carbon	-5.5
Magnesium ...	-10.4
Calcium	-12
Iron..............	-10.7

FIG. 10.—Energy distributions for several models at $T_{eff} = 7700$ K and $\log g = 8.0$: a pure helium model (*dotted line*); a model with traces of carbon ($\log[C/He] = -5.5$; *thick solid line*); and a model with the same traces of carbon, but without the carbon opacity included (*thin solid line*). There is a significant shift in the peak of the energy distribution of the models that include traces of carbon, which appear bluer than their carbon-free counterparts.

that a model with a higher effective temperature will be required if pure helium models are used instead of models with traces of carbon. The lowering of the best-fit temperature when models including carbon are used is clearly related to the traces of heavy elements present in the atmosphere, but in a somewhat convoluted way. We find that the presence of additional atmospheric constituents is felt principally through the equation of hydrostatic equilibrium. The slight change in opacity due to carbon's presence leads to a reduction of the convective flux. The accompanying steepening of the radiative gradient, required to get the energy out of the photosphere, leads to an energy distribution that appears bluer than it would were carbon not present.

5. DISCUSSION

5.1. *The Radius of Procyon B*

As discussed above, the effective temperature of and solid angle subtended by Procyon B are determined by fitting the energy distribution reconstructed in § 2. The stellar radius is obtained by combining the optimal value of Ω with the measured parallax. The fit yields $T_{eff} = 7740$ K and $\Omega = 1.989 \times 10^{-20}$ sr for Procyon B. At a distance of 3.50 pc, the associated stellar radius is $R = 0.01234 \, R_\odot$.

We are now interested in understanding the contributions of different uncertainties in our analysis to the overall radius error. On the basis of equation (2), the error in radius is a combination of the errors in parallax and solid angle. The former is given by Girard et al. (2000), $\pi = 285.9 \pm 0.9$ mas, which yields $\Delta\pi/\pi = 0.0031$. The latter, as well as the error in T_{eff}, is a function of (1) the formal uncertainty of the fitting parameters, which depends on the spectrum's S/N ratio and on the ability of our models to correctly reproduce the spectral shape, (2) the uncertainty associated with the correction factor f, and (3) the uncertainty of Procyon B's photospheric carbon abundance. On the basis of various experiments we carried out, including varying f from 0.88

to 0.95 (Fig. 11), we estimate that the following errors are associated with each of these three sources: $\Delta T_{eff} = 27$ K and $\Delta\Omega/\Omega = 0.0111$ for the formal fitting uncertainty; $\Delta T_{eff} = 25$ K and $\Delta\Omega/\Omega = 0.0486$ for the f-factor; and $\Delta T_{eff} = 37$ K and $\Delta\Omega/\Omega = 0.0130$ for the C/He abundance. The combination of these three sources of error, which are considered statistically independent, yields $\Delta T_{eff} = 52$ K, as well as $\Delta\Omega/\Omega = 0.0515$.

The final error in radius is determined from equation (2) by applying standard error propagation techniques, under the assumption of statistical independence of the sources of uncertainty:

$$\frac{\Delta R}{R} = \left[\left(\frac{1}{2}\frac{\Delta\Omega}{\Omega}\right)^2 + \left(\frac{\Delta\pi}{\pi}\right)^2\right]^{1/2}. \qquad (3)$$

We find $\Delta R/R = 0.0259$, or $\Delta R = 0.00032 \, R_\odot$. The error budget is dominated by the uncertainty associated with the lack of internal consistency of the STIS photometric calibration. The uncertainty of the photospheric carbon abundance and the fitting uncertainties lag farther behind, followed by the error of the parallax. There is hope that the remaining error in stellar radius can be brought farther down once the residual calibrations problems are addressed.

Table 3 and Figure 12 present the current observational support for the white dwarf mass-radius relation, using white dwarfs in the three well-studied visual binaries. While the number of observed data points is indeed sparse, the agreement between theory and observation is encouraging. Sirius B, a DA white dwarf, is within 1.5 σ of the thick hydrogen atmosphere ($\log M_H = -4$), 25,000 K Wood (1995) model. As discussed in Provencal et al. (1998), 40 Eri B, classified as a DA, probably has a thin hydrogen atmosphere. The location of this object is more appropriately compared with model sequences containing no hydrogen envelope. According to Figure 12, the 40 Eri B point lies within 1 σ of the 16,700 K model with $M_H = 0$. Procyon B is now known to possess a helium-dominated atmosphere, and its position is within 1 σ of both the zero-temperature Hamada & Salpeter (1961) relation for a carbon core and the Wood (1995) model with $M_H = 0$.

5.2. *Origin of the Heavy Elements*

The canonical explanation for the existence of heavy elements in the atmospheres of cool white dwarfs is a combination of episodic accretion from the interstellar medium and element separation arising from downward diffusion of heavy metals (Dupuis, Fontaine, & Wesemael 1993). Heavy elements found in any cool white dwarf cannot be primordial. The timescale for a white dwarf to cool to 7800 K, for example, is about 2×10^9 yr (Wood 1995), much longer than the estimated diffusion timescale of 10^6 yr.

For reasons that remain unknown, stars of spectral type DQZ are quite rare among field white dwarfs (Bergeron et al. 2001). Therefore, it is tempting to assume that the magnesium, calcium, and iron features observed in the spectrum of Procyon B are linked to the proximity of Procyon A, rather than to normal accretion from the interstellar medium or to some form of convective dredge-up, the generally assumed origin of photospheric carbon in DQ stars.

Our own Sun loses approximately $10^{-14} \, M_\odot$ yr^{-1}. The solar wind originates in the hot corona and consists of electrons, protons, and ionized heavier elements. Procyon A is
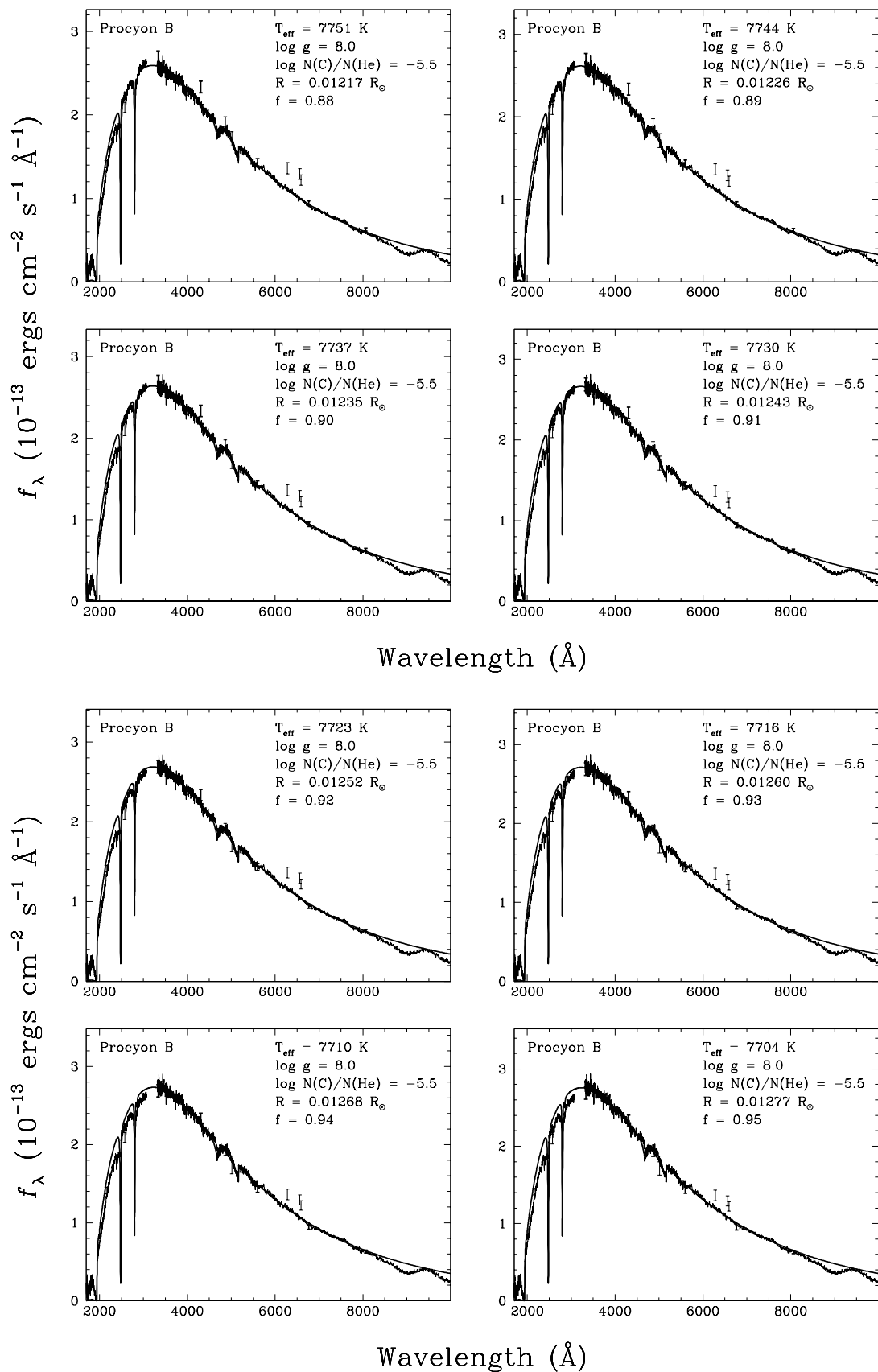
FIG. 11.—An investigation into the dependence of temperature and radius on the gray scale factor *f*. It is clear that *f* lies between 0.89 and 0.92. Our best fit to all parameters is obtained using *f* = 0.90.

TABLE 3
WHITE DWARFS IN VISUAL BINARIES

Parameter	Procyon B	Sirius B	40 Eri B	Stein 2051B
Mass ($M_\odot$)	0.602 ± 0.015	1.034 ± 0.026	0.501 ± 0.011	0.66 ± 0.04[a]
m_v	10.82 ± 0.03	8.44 ± 0.06	9.50 ± 0.02	12.43 ± 0.1
T_{eff} (K)	7740 ± 50	24790 ± 100	16700 ± 300	7100 ± 300
π (mas)	285.9 ± 0.9	379.21 ± 1.58	198.24 ± 0.84	180.6 ± 0.8
Radius ($R/R_\odot$)	0.01234 ± 0.00032	0.0084 ± 0.00025	0.0136 ± 0.0002	0.011 ± 0.001
Error Budget:				
$\Delta\Omega/\Omega$	0.0515	. . .	. . .	. . .
$\Delta f_\lambda/2f_\lambda$	. . .	0.0235	0.01	0.047
$\Delta H_\lambda/2H\lambda$	. . .	0.0107	0.009	0.07
$(\Delta\pi/\pi)$	0.0031	0.0042	0.005	0.005
Net Error $\Delta R/R$	0.026	0.026	0.014	0.085

[a] Stein 2051B's mass is a spectroscopic determination, not from the binary orbit.

REFERENCES.—Girard et al. 2000 (Procyon B); Holberg et al. 1998 (Sirius B); Shipman et al. 1997 (40 Eri B); Bergeron et al. 2001 (Stein 2051B).

known to have a corona dominated by material with $T_{\mathrm{cor}} \sim 1.6 \times 10^6$ K and an inferred volume of $\sim 5 \times 10^{31}$ cm^3 (Schmidt et al. 1996). It might be possible to use the atmosphere of Procyon B as a probe of the stellar wind of its primary.

We use the information in Dupuis et al. (1993) to estimate the accretion rate required to produce the heavy-element abundances observed in the atmosphere of Procyon B. The assumption of accreting material of solar abundance is well
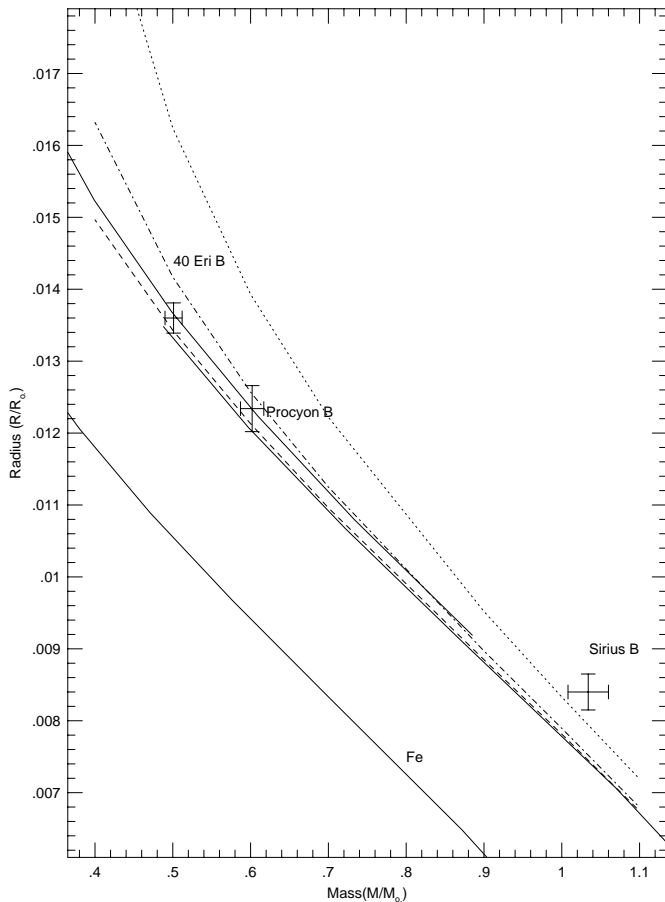

FIG. 12.—Same as Fig. 1, but for revised positions of Procyon B, Sirius B, and 40 Eri B. Stein 2051B is not included because its mass is a spectroscopic determination, not derived from the binary orbit.

justified here. Faraggiana et al. (1986) indicate that the abundances of metals in the atmosphere of Procyon A are, with few exceptions, solar. This result is confirmed by the near-infrared analysis of Kato, Watanabe, & Sadakane (1996). Identified features in the ultraviolet spectrum of Procyon A include Mg I, Mg II, C I, Fe I and Fe II, and Ca H and K.

Interestingly, we find similar accretion rates of $\sim 2 \times 10^{-19}$ $M_\odot$ yr^{-1} for the three heavy elements that we assume are accreted in Procyon B's atmosphere, namely, Mg, Ca, and Fe. In addition, the observed abundance ratios of Mg/Ca, Fe/Ca, and Fe/Mg are consistent with solar abundances, as described in Table 3 of Dupuis et al. (1993).

Unfortunately, the geometry of the stellar wind emanating from Procyon A is unknown and probably departs significantly from spherical symmetry. Nevertheless, within the framework of that simplifying assumption, we infer an upper limit for Procyon A's mass-loss rate of 10^{-7} $M_\odot$ yr^{-1}. Further investigation of this interesting question is beyond the scope of this paper.

5.3. The Progenitor of Procyon B

The chemical evolution of galactic material merges our understanding of stellar evolution, nucleosynthesis, star formation, and galaxy evolution. The initial-final mass relationship constrains the total amount of mass lost by a star during its evolution. The lost mass, enriched with processed material, is returned to the interstellar medium, where it provides the raw material for the next generation of stars.

The Procyon system is an important test case for the initial-final mass relationship. Provencal et al. (1998) estimated the mass of Procyon B's progenitor as 1.7 $M_\odot$. Given our revision of the white dwarf's temperature and our firm belief that Procyon B does have a carbon core, we reinvestigate this issue.

The final mass of Procyon B is well known, $M_B = 0.602 \pm 0.015$ $M_\odot$ (Girard et al. 2000). Because the progenitor itself is long gone, we must infer its mass from the properties of the Procyon system. Many studies examining the upper mass limit for white dwarf formation investigate stellar clusters, where the age of the stellar ensemble can be determined from the cluster turnoff point. We can think of Procyon A and B as a cluster with two members and base our age determination on the observation that

Procyon A is leaving the main sequence (Lachaume et al. 1999; Guenther & Demarque 1993). Girard et al. (2000) determine a mass for Procyon A, based on over 250 photographic plates spanning 83 yr, of $M_A = 1.497 \pm 0.037\ M_\odot$. The main-sequence lifetime of Procyon A is therefore approximately 3×10^9 yr. The cooling age for a carbon core, helium atmosphere white dwarf with $T_{eff} = 7740$ K is approximately $(1.7 \pm 0.1) \times 10^9$ yr (Wood 1995). Subtracting the cooling age from Procyon A's main-sequence lifetime leaves a main-sequence lifetime for the white dwarf progenitor of 1.3×10^9 yr. This in turn indicates a progenitor mass of $\sim 2.1\ M_\odot$.

6. CONCLUSIONS

We have successfully used the unique abilities of *HST* to obtain a nearly complete spectrum of Procyon B. The STIS spectrum confirms the Provencal et al. (1997) suggestion of a helium atmosphere. However, the data also reveal the presence of carbon, magnesium, calcium, and iron in the atmosphere of Procyon B. The electrons contributed by these heavy elements influence the opacity of the helium atmosphere and our effective temperature determination. We find $T_{eff} = 7740 \pm 50$ K, a value lower than that reported by Provencal et al. (1997). The lower temperature in turn implies a larger stellar radius. We find $R = 0.01234 \pm 0.00032\ R_\odot$, a value that agrees well with the predictions of Hamada & Salpeter (1961) and Wood (1995) for carbon cores. We have found our way out of the iron box.

The simultaneous presence of carbon and other heavy elements in the helium-rich atmosphere of a cool white dwarf is a rare occurrence. We speculate that this situation may be linked to the proximity of the white dwarf to Procyon A. The derived abundances of Mg, Ca, and Fe indicate an accretion rate of $2 \times 10^{-19}\ M_\odot$ yr^{-1}, assuming solar abundances for the accreted material. Procyon B may thus prove to be a valuable probe of the stellar wind of its primary. We also reconsider the issue of the initial-final mass relation. Because Procyon A is leaving the main sequence, we use the star's nuclear lifetime to limit the system age. Incorporating the white dwarf cooling times of Wood (1995), we find a progenitor mass for the white dwarf of $\sim 2.1\ M_\odot$.

Procyon B is an interesting and important object deserving continued attention. The next steps in our investigation should include further reduction of the error bar in radius, since a large portion of the radius error originates with the internal inconsistency of the calibrated fluxes. Clearly, our exploration of stellar degeneracy is far from complete. Figure 13 shows the current observational support for the white dwarf mass-radius relation, based on the positions of visual binaries, common proper motion systems and field white dwarfs. The sample includes the four white dwarfs in visual binaries (*extra-thick error bars*), seven white dwarfs in common proper motion systems with gravitational redshift masses (*thick error bars*), and 10 field white dwarfs with masses determined through spectroscopic analysis (*thin error bars*). While Table 3 shows that the remaining radius errors in the visual binaries lie in uncertainties in flux and temperature, parallax dominates the error for the common proper motion systems. Unlike those for visual binaries or
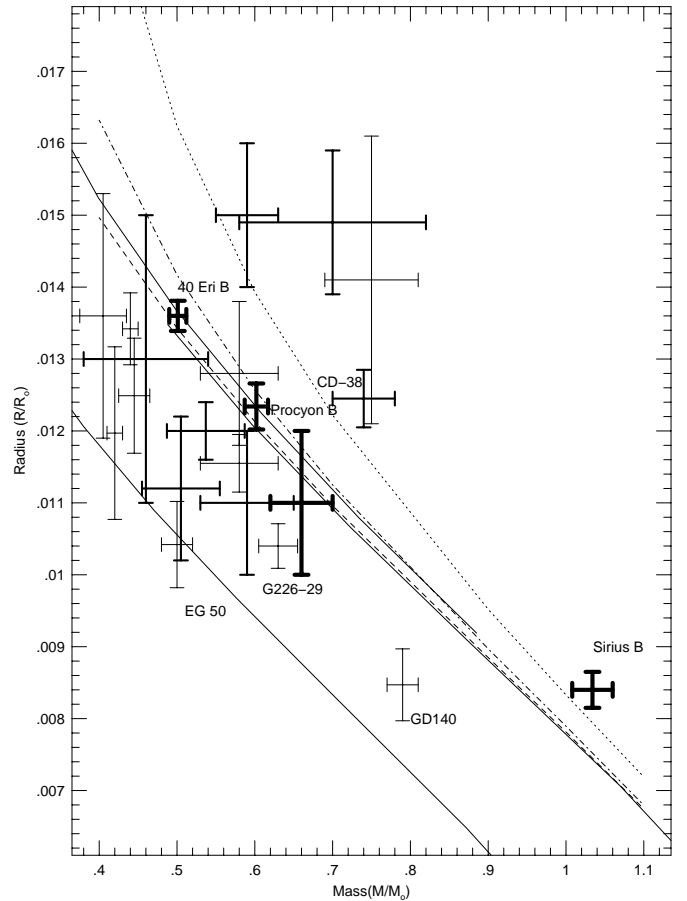

FIG. 13.—Same as Fig. 1, but for current observational support. Positions of the visual binaries Procyon B, Sirius B, 40 Eri B, and Stein 2051B (*extra-thick error bars*), common proper motion systems (*thick error bars*), and field white dwarfs (*thin error bars*) are shown.

common proper motion systems, mass determinations for field white dwarfs are indirect, relying on comparison of observed spectra with detailed model atmosphere predictions (see Provencal et al. 1998 for a detailed discussion). Our future work will focus on further reduction of error bars for all types of objects. We can gain additional precision by improving orbital parameters, effective temperatures, surface gravities, magnitudes, and atmospheric models. We also hope to add new points to Figure 13. Analysis of the white dwarf binary G107-70 is currently underway.

REFERENCES

Bergeron, P. Leggett, S. K., & Ruiz, M. T. 2001, ApJS, 133, 413
Bergeron, P., Ruiz, M. T., & Leggett, S. K. 1997, ApJS, 108, 339
Bergeron, P., Saumon, D., & Wesemael, F. 1995, ApJ, 443, 764
Chandrasekhar, S. 1933, MNRAS, 93, 390
Dupuis, J., Fontaine, G., & Wesemael, F. 1993, ApJS, 87, 345
Faraggiana, R., Castelli, F., Morossi, C., Kondo, Y., & van der Hucht, K. A. 1986, ApJS, 61, 719
Finley, D. S., Koester, D., & Basri, G. 1997, ApJ, 488, 375
Girard, T. M., et al. 2000, AJ, 119, 2428
Guenther, D. B., & Demarque, P. 1993, ApJ, 405, 298
Hamada, T., & Salpeter, E. E. 1961, ApJ, 134, 683
Holberg, J. B., Barstow, M. A., Bruhweiler, F. C., Cruise, A. M., & Penny, A. J. 1998, ApJ, 497, 935
Kato, K., Watanabe, Y., & Sadakane, K. 1996, PASJ, 48, 601
Koester, D., Weidemann, V., & Zeidler-K. T., E.-M. 1982, A&A, 116, 147
Koester, D., & Wolff, B. 2000, A&A, 357, 587
Kurucz, R. L., & Bell, B. 1995, CD-ROM No. 23, Atomic Line List (Cambridge: SAO)

Lachaume, R., Dominik, C., Lanz, T., & Habing, H. J. 1999, A&A, 348, 897
Press, W. H., Flannery, B. P., Teukolsky, S. A., & Vetterling, W. T. 1986, Numerical Recipes (Cambridge: Cambridge Univ. Press)
Provencal, J. L., Shipman, H. L., Høg, E., & Thejll, P. 1998, ApJ, 494, 759
Provencal, J. L., Shipman, H. L., Wesemael, F., Bergeron, P., Bond, H. E., Liebert, J., & Sion, E. M. 1997, ApJ, 480, 777
Schmidt, J. H. M. M., Drake, J. J., Haisch, B. M., & Stern, R. A. 1996, ApJ, 467, 841
Shipman, H. L., & Provencal, J. L. 1999, in ASP Conf. Ser. 169, 11th European Workshop on White Dwarfs, ed. J.-E. Solheim & E. G. Meištas (San Francisco: ASP), 15
Shipman, H. L., Provencal, J. L., Høg, E., & Thejll, P. 1997, ApJ, 488, L43
Walker, G. A., Walker, A. R., Racine, R., Fletcher, J. M., & McClure, R. D. 1994, PASP, 106, 356
Wehrse, R., & Liebert, J. 1980, A&A, 86, 139
Wood, M. A. 1995, in 9th European Workshop on White Dwarfs, ed. D. Koester & K. Werner (Berlin: Springer), 41
Zeidler-K. T., E.-M., Weidemann, V., & Koester, D. 1986, A&A, 155, 356